e-ISSN: 2550-164X

Available online at
https://jmeche.uitm.edu.my/browse-journals/regular-issue/regular-issue-2025-vol-22-3/

Journal of Mechanical Engineering 22(3) 2025, 111 – 119.

Journal of Mechanical Engineering

Transforming Fish Bone Waste into Hydroxyapatite: Insights into Heating Rate Influences During Calcination

M. R. H. Mohd Nasir[1], C. M. Mardziah[1*], N. M. Nik Rozlin[1], M. K. Abbas[2]

[1]*Faculty of Mechanical Engineering, Universiti Teknologi MARA, 40450 Shah Alam, Selangor, Malaysia*
[2]*Centre for Advanced Materials (CAM), Qatar University, P.O. Box 2713, Doha, Qatar*

ARTICLE INFO

Article history:
Received 15 May 2025
Revised 22 July 2025
Accepted 28 July 2025
Online first
Published 15 September 2025

Keywords:
Calcination process
Heating rate
Fish bone wastes
Hydroxyapatite
Microstructural modification

DOI:
https://doi.org/10.24191/jmeche.v22i3.6477

ABSTRACT

In recent years, the exploration of hydroxyapatite (HA) derived from natural resources has witnessed an exponential growth, surpassing the attention given to its synthetic counterparts. Fish bone waste, typically generated from the seafood industry, is often discarded in landfills, which contributes to environmental pollution. Despite its high calcium content, fish bone is still underutilised as a raw material for producing HA. In this study, HA was synthesised via calcination at 1000 °C while heating rates were varied at 2 °C/min and 5 °C/min. The purpose of this study is to produce HA powders from fish bone wastes (HA-fb) and to examine how its characteristics would be affected by altering the heating rate during thermal treatment Thermogravimetric curve revealed a few definite stages of weight loss, mainly due to water evaporation and inorganic compound removal as the temperature increases. XRD analysis demonstrated the appearance of prominent HA and β-TCP peaks in both samples, a typical observation in naturally derived HA powders. In addition, FTIR spectra displayed the emergence of functional groups for hydroxyl, phosphate, and carbonate, further affirming HA formation. FESEM analysis revealed that powders produced at higher heating rates exhibited larger particle sizes and greater agglomeration compared to those synthesised at slower heating rates, confirming the microstructural modification due to the use of different heating rates. The findings from this study would provide valuable information about the effect of exploiting heating rates during the calcination process, particularly on the morphology of the HA-fb powder particles.

INTRODUCTION

Hydroxyapatite (HA), a prominent biomaterial with a rich history, has undergone a remarkable evolution, transitioning from a basic biocompatible substance to a sophisticated functional material with diverse applications (Mondal et al., 2023). In its crystalline state, HA [$Ca_{10}(PO_4)_6(OH)_2$] exhibits thermodynamic

[1*] Corresponding author. *E-mail address*: mardziah31@uitm.edu.my
https://doi.org/10.24191/jmeche.v22i3.6477

stability in body fluids, closely resembling the composition of bone mineral. As the primary inorganic component of human bone and teeth, HA assumes a critical role in hard tissue engineering, distinguished by its exceptional biocompatibility and bioactivity when compared to alternative materials (Fendi et al., 2024). Its prevalence in the biomedical field is marked by widespread use owing to its compatibility and likeness to native human bone apatite (Radulescu et al., 2023). Advances in material synthesis and engineering have propelled HA into diverse disciplines, as researchers have adeptly tailored its composition, morphology, and surface characteristics. Although there are multiple techniques available for synthesising HA, their applicability is constrained by economic and performance factors. Challenges arise from intricate processes, significant aggregation, as well as the presence of contaminants. One such approach is to obtain HA from natural sources, which helps overcome the limits of synthetic techniques (Hartati et al., 2022).

HA synthesis can be achieved through chemical means using specific reagents or naturally through the utilisation of calcium sources obtained from natural reservoirs. The chemical synthetic route offers precise control over the morphology, crystallinity, and stoichiometric composition of the resulting HA. Chemically synthesised HA typically exhibits a reduced crystal size, resulting in a larger surface area (Mohd Pu'ad et al., 2020). However, these synthetic approaches are characterised by their high cost, complexity, and time-consuming process, ultimately yielding HA with constrained biological performance (Toibah et al., 2019; Ramesh et al., 2018; Ofudje et al., 2018). In contrast, HA derived from natural sources possesses the necessary physicochemical properties, and notably, it promotes cell proliferation without exhibiting cytotoxic effects, a characteristic not observed in samples prepared using chemical precursors (Kumar et al., 2021; Barua et al., 2019).

Natural waste serves as valuable resources for HA extraction, requiring specific techniques for transforming them into functional materials (Rahavi et al., 2017). Naturally derived apatites, termed carbonated apatite or carbonate apatite, contain minor substituents such as CO_3^{2-}, Na^+, Mg^{2+}, setting them apart from pure HA (Mohd Pu'ad et al., 2019). Fish bones, scales, and shells, as well as limestone and dolomite, are alternative sources rich in calcium and phosphate, fundamental components of HA (Mohd Pu'ad et al., 2019). The escalating global demand for fisheries and aquaculture production, reaching a staggering 179 million tonnes in 2018 from 19 million tonnes in 1950, signifies a remarkable growth trend over the past seven decades (Laonapakul et al., 2021). However, a substantial portion of this harvest, ranging between 50% and 60%, transforms into underutilised solid waste, characterised by low added value (Paul et al., 2017). This aquatic waste comprises organic collagen and inorganic HA, with reported HA recovery yields falling between 50% and 53% (Granito et al., 2018). Recognizing this untapped resource, the focus shifts to the unique properties of fish scales and bones. While HA production from animal bones like bovine is well-studied, fish bone waste remains underexplored. The abundance of bio-calcium in fish bones (Arkanit et al., 2025), known for its biocompatibility and non-toxic nature, positions it as a potential biomaterial, particularly for constructing bone scaffolds (Fendi et al., 2023). Furthermore, utilising waste is economically advantageous, aligns with sustainable and environmentally friendly practices (Mesri et al., 2023).

In this present study, the synthesis of fish bone-derived HA (HA-fb) involved carefully planned procedures, starting with sourcing fish bones from reliable outlets and subjecting them to a series of steps, including cleaning, drying, and grinding to obtain finely powdered fish bones. Following the grinding process, the powdered fish bones underwent thermal calcination at 1000 °C to convert them into crystalline HA-fb. Unlike previous studies that focused solely on calcination temperatures, this work investigates the effect of varying heating rates during the calcination process. The main objective of this study was to examine how using different heating rates (2 °C/min and 5 °C/min) during calcination would affect the chemical and physical properties of HA-fb powders.

https://doi.org/10.24191/jmeche.v22i3.6477

METHODOLOGY

Collection, Cleaning, and Drying of Fish Bones

The synthesis of HA-fb involves a carefully planned procedure. Fish bones, chosen for their availability and compositional similarity to human bones, were sourced from reliable outlets such as surplus fish remains or bones obtained from local restaurants and fish markets. The sample of fish bone waste that had been collected is shown in Fig 1(a). To initiate the extraction process, any residual meat attached to the bones was carefully removed using a knife to minimize impurities and undesired organic matter. The cleaned fish bones were subsequently cleaned in boiling water before undergoing a drying process for 24 hours at 100 °C in an oven. This drying step is crucial for obtaining bone fragments with optimal properties, facilitating subsequent processing.

Fig. 1. (a) Collected fish bones and (b) crushed fish bones.

Calcination of Dried and Crushed Fish Bones

Once fully dried, the fish bones were crushed into small pieces using a blender. This crushing process was designed to break down the bones into smaller fragments (shown in Fig 1(b)), enhancing the surface area available for chemical reactions.

Fig. 2. HA-fb white powders obtained after the calcination process.

The resulting crushed fish bone fragments serve as a suitable starting material for the subsequent calcination process. The crushed bones were heated in the conventional furnace for two hours at 1000 °C using different heating rates of 2 °C/min and 5 °C/min for comparison. The resulting powders (shown in Fig 2) were observed to be white in colour, indicating the successful formation of HA-fb.

https://doi.org/10.24191/jmeche.v22i3.6477

Characterisation Methods

The characterisation of HA-fb was performed using several analytical methods, such as thermogravimetric (TG) analysis, X-ray diffraction (XRD), Fourier transform infra-red (FTIR), and field emission scanning electron microscopy (FESEM). Thermal stability and decomposition of dried raw fish bone were studied by a TG analyser (Mettler Toledo) from 25 °C to 1000 °C at an average heating rate of 5 °C/min. The presence of HA and β-TCP was determined using the XRD (Rigaku Model Ultima IV) over a 2θ range from 20° to 60°. The functional groups and main chemical compositions in both samples, calcined at different heating rates of 2 °C/min and 5 °C/min were analysed by FTIR (PerkinElmer, Spectrum One), ranging from 500 cm^{-1} to 4000 cm^{-1}. The morphology analysis and particle sizes of the powder samples were studied by FESEM, which provides high-resolution images of the surface morphology of HA-fb.

RESULTS AND DISCUSSION

Thermogravimetric (TG) Analysis

The TG curve in Fig 3 shows the weight loss of dried raw fish bones within the 25 °C to 1000 °C temperature range. It should be noted that the initial weight of dried raw fish bone was measured at 13.5 mg. The first stage of weight loss was 5.26% which occurred starting from 25 °C until 218.5 °C due to the evaporation of water (Mardziah et al., 2021; Boudreau et al., 2025). In stage 2, the weight loss of 26.15% took place at around 218.5 °C to 479.8 °C indicates the decomposition of organic materials or volatile components such as fats and collagen (Mardziah et al., 2021). The result is similar to the one reported by other researchers (Hussin et al., 2023), which stated that the weight loss that occurred at around 332 °C was attributed to the removal of adsorbed water and part of the organic component. In the final stage, the weight loss was calculated as 10.18% which occurred at approximately 479.8 °C to 850 °C, involving further decomposition of HA, leading to its formation into another phase, β-TCP. Finally, the curve reaches its plateau stage at around 850 °C, indicating no subsequent phase changes and signifying the thermal stability of HA-fb at this temperature.

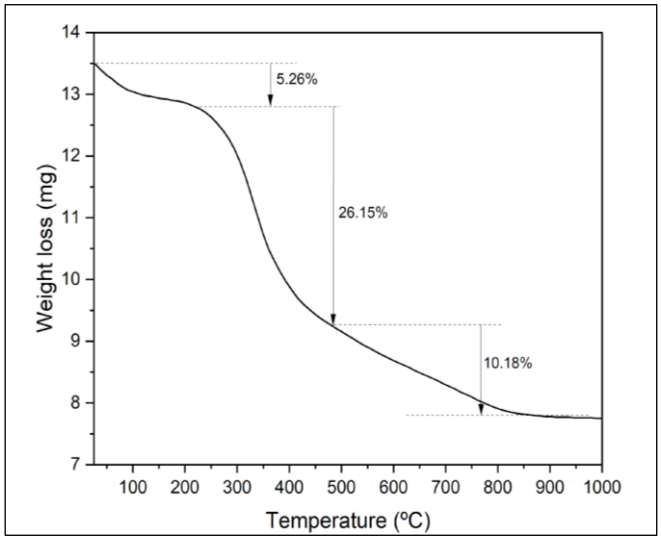

Fig. 3. TG curve of dried raw fish bones heated at 5 °C/min.

https://doi.org/10.24191/jmeche.v22i3.6477

X-Ray Diffraction (XRD) Analysis

Diffraction positions of the peaks in XRD analysis demonstrated in Fig 4 were indexed to HA and β-TCP in both samples, in accordance with the ICCD Card No. 00-025-0166 and 00-055-0898, respectively. The peak observed at approximately 2θ = 31.8° in both samples is one of the most intense and distinct reflections for HA, indicating the formation of a highly ordered crystalline structure. The other two peaks that reflect the formation of HA were detected at around 32° and 32.2°. The consistent peak intensity suggests that the calcination heating rates did not significantly affect the crystallinity of HA, maintaining its primary crystal structure. However, the higher heating rate leads to a slightly intense HA peak, suggesting better crystallinity but still results in the β-TCP formation despite a more rapid thermal treatment. Furthermore, the sample calcined at 2 °C/min produced a higher peak of β-TCP, indicating reduced phase stability attributed to the thermal decomposition of HA.

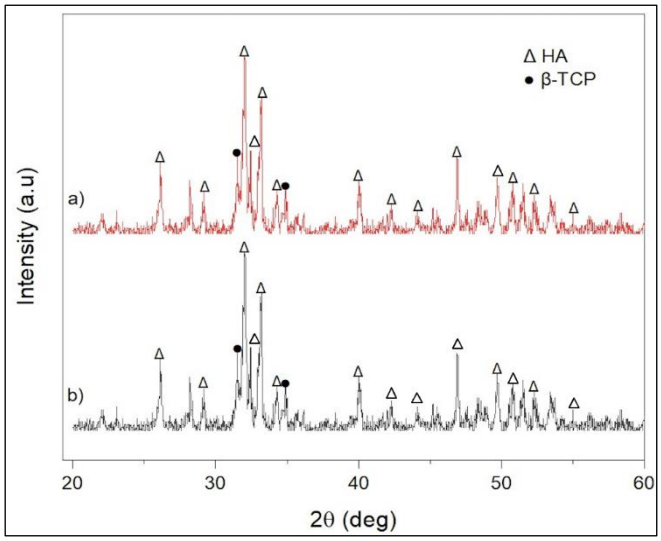

Fig. 4. XRD patterns of (a) HA_{fb}-5 °C/min and (b) HA_{fb}-2 °C/min powders calcined at 1000 °C.

However, these differences are barely noticeable from the XRD patterns, therefore can be considered as insignificant. This result is in contrast to the findings of Sunil & Jagannatham (2016), who reported that no peaks corresponding to β–TCP were detected from 600 °C to 1000 °C in their XRD analysis. They attributed this to the fact that the HA-fb they developed did not belong to the calcium-deficient HA family. On the other hand, the lattice parameters a and c of the sample calcined at 5 °C/min heating rate are somewhat larger (a=9.3968 Å, c=6.8666Å) compared to the sample calcined at 2 °C/min (a=9.3731Å, c=6.8595Å). The slight difference in lattice parameter variations was most likely attributed to thermal expansion occurring at a higher heating rate, which is in agreement with other work reported by Londoño-Restrepo et al. (2019).

Fourier Transform Infra-Red (FTIR) Analysis

Fig 5 demonstrates the FTIR spectra of different calcined powders. These samples show regular vibrational modes correlated with the hydroxyl (OH), carbonate (CO_3), and phosphate (PO_4), in accordance with the functional groups found in the HA structure (Kjidaa et al., 2024; Hammal et al., 2024). Both spectra display minor differences only despite different heating rates, indicating that the heating rate effect is considered minimal on the HA molecular structure. The presence of OH can be spotted in both samples in two modes, including in liberation mode at 630 cm^{-1} and stretching mode at around 3570 cm^{-1}, suggesting

https://doi.org/10.24191/jmeche.v22i3.6477

the presence of water or hydroxylated compound associated with HA characteristics. For the sample calcined at 5 °C/min, the CO_3 group appeared at 1460 cm^{-1}, most likely due to the slightly rapid heating rate. In addition, HA structure related to PO_4 functional group was identified in four various vibrational modes (v_1-symmetric stretch, v_2-bending, v_3-asymmetric stretching and v_4-bending), spotted at 560 cm^{-1} (v_2), 600 cm^{-1} (v_4), 965 cm^{-1} (v_1) and around 1024-1088 cm^{-1} (v_3) wavenumbers (Mohd Pu'ad et al., 2019). The intensity of PO_4 and OH peaks is almost similar in both samples, signifying that the heating rate has a negligible effect on altering the molecular structure of HA.

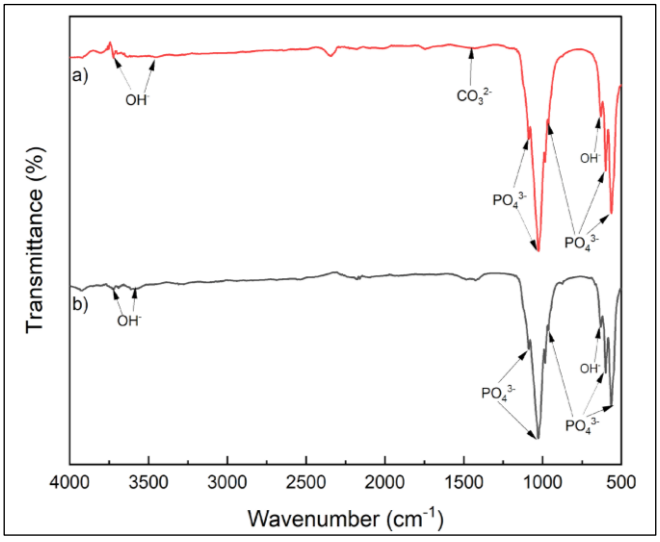

Fig. 5. FTIR spectra of (a) HA_{fb}-5 °C/min and (b) HA_{fb}-2 °C/min powders calcined at 1000 °C.

Field Emission Scanning Electron Microscopy (FESEM) Analysis

FESEM images in Fig 6 show the morphology of the synthesised HA-fb powders, highlighting significant variations in the morphology and particle size between the two samples. The sample calcined at a higher heating rate (5 °C/min) produced a larger particle size by nearly double (0.42±0.074 µm) compared to the sample calcined at 2 °C/min (0.25±0.092 µm), probably due to longer thermal energy exposure. The sample calcined at a slower heating rate appears to be in a rod-like shape with smaller and less agglomerated particles, making more surface sites available for reactions, adsorption, or other interactions.

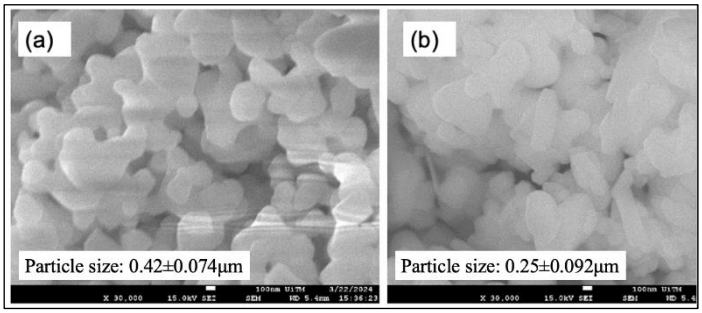

Fig. 6. FESEM images of (a) HA_{fb}-5 °C/min and (b) HA_{fb}-2 °C/min powders calcined at 1000 °C.

https://doi.org/10.24191/jmeche.v22i3.6477

FESEM analysis reported by Gnabasekaran et al. (2024), on the contrary, showed that the HA-fb particles displayed a spherical morphology, with a much smaller average particle size between 50 nm and 80 nm. This is likely the result of the extended soaking time (5 hours) used during the calcination process. Other researchers (Hussin et al., 2023) claimed that the shape of the HA-fb powders was found to be spherical and hexagonal shape after calcination at 600 °C, 900 °C, and 1200 °C. In this present study, we discovered that the sample calcined at a faster heating rate appears to be in greater agglomeration and clustered together, exhibiting lower overall surface area. It is clear that the impact of different heating rates during calcination provides the most notable effect, specifically on the morphology and size of the HA-fb powder particles.

CONCLUSIONS

In the present study, HA-fb powders were synthesised using fish bone waste through a direct calcination method. TG analysis indicates the total weight loss of dried fish bone was ~42.2% which occurred at a few stages due to evaporation, dehydration, and decomposition of organic materials. XRD analysis reveals prominent HA peaks at approximately 31.8°, 32°, and 32.2°, indicating that both powders were highly crystalline. Sample calcined at 5 °C/min shows only slightly more β-TCP formation due to decomposition of HA-fb. FTIR spectra display typical vibrational modes inherent to the HA structure for both samples. The appearance of a less intense peak belongs to the CO_3 group in the sample calcined at 2 °C/min indicates slightly lower crystallinity powder than the one calcined at a higher rate. Among all analyses, FESEM evaluation reveals the most prominent difference due to the application of different heating rates. Sample calcined at 5 °C/min produced larger agglomeration, more spherical-shaped particles. On the contrary, the sample calcined at a slower heating rate reveals minimal agglomeration and smaller rod-like shaped particles. The morphological differences in particle shape and size proved that heating rate during thermal treatment can be manipulated according to specific requirements, especially for biomedical applications.

ACKNOWLEDGEMENTS/ FUNDING

The authors would like to thank the Ministry of Higher Education Malaysia (MOHE) for the research fund provided under the Fundamental Research Grant Scheme (FRGS), No.: FRGS/1/2023/TK09/UITM/02/2.

CONFLICT OF INTEREST STATEMENT

The authors agree that this research was conducted in the absence of any self-benefits, commercial or financial conflicts, and declare the absence of conflicting interests with the funders.

AUTHORS' CONTRIBUTIONS

The authors confirm their contribution to the paper as follows: conceptualization, supervision, validation, writing-review and editing: C. M. Mardziah; methodology and writing-original draft preparation: M. R. H. Mohd Nasir; writing-review and editing: N. M. Rozlin; review and editing: M. K. Abbas. All authors reviewed the results and approved the final version of the manuscript.

https://doi.org/10.24191/jmeche.v22i3.6477

REFERENCES

Arkanit, K., Senphan, T., Issapap, N., Mungmueang, N., Sriket, P., Benjakul, S., & Sriket, C. (2025). Physicochemical properties and bioavailability of bio-calcium products from tilapia bone: A comparative study with synthetic hydroxyapatite. Journal of Agriculture and Food Research, 19, 101708.

Barua, E., Das, A., Pamu, D., Deoghare, A. B., Deb, P., Lala, S. D., & Chatterjee, S. (2019). Effect of thermal treatment on the physico-chemical properties of bioactive hydroxyapatite derived from caprine bone bio-waste. Ceramics International, 45(17), 23265-23277.

Boudreau, S., Hrapovic, S., McIsaac, E., Lam, E., Berrue, F., & Kerton, F. M. (2025). Transforming waste fish bones into nanoparticles with ultrasound and aqueous organic acids. RSC Sustainability, 3(5), 2325-2332.

Fendi, F., Abdullah, B., Suryani, S., Raya, I., Usman, A. N., & Tahir, D. (2023). Hydroxyapatite derived from fish waste as a biomaterial for tissue engineering scaffold and its reinforcement. AIP Conference Proceedings, 2719(1), 020040.

Fendi, F., Abdullah, B., Suryani, S., Usman, A. N., & Tahir, D. (2024). Development and application of hydroxyapatite-based scaffolds for bone tissue regeneration: A systematic literature review. Bone, 183, 117075.

Gnanasekaran, R., Yuvaraj, D., Muthu, C. M. M., Ashwin, R., Kaarthikeyan, K., Kumar, V. V., Ramalingam, R. J., Al-Lohedan, H., & Reddy, K. (2024). Extraction and characterization of biocompatible hydroxyapatite (HAp) from red big eye fish bone: Potential for biomedical applications and reducing biowastes. Sustainable Chemistry for the Environment, 7, 100142.

Granito, R. N., Renno, A. C. M., Yamamura, H., de Almeida, M. C., Ruiz, P. L. M., & Ribeiro, D. A. (2018). Hydroxyapatite from fish for bone tissue engineering: A promising approach. International Journal of Molecular and Cellular Medicine, 7(2), 80-90.

Hammal, A., Al-Duihi, H. A. H., & Alchab, L. (2024). Preparation of nano hydroxyapatite loaded with syrian inula extract against dental caries. Materials Chemistry and Physics, 327, 129872.

Hartati, Y. W., Irkham, I., Zulqaidah, S., Syafira, R. S., Kurnia, I., Noviyanti, A. R., & Topkaya, S. N. (2022). Recent advances in hydroxyapatite-based electrochemical biosensors: Applications and future perspectives. Sensing and Bio-Sensing Research, 38, 100542.

Hussin, M. S. F., Idris, M. I., Abdullah, H. Z., Azeem, W., & Ghazali, I. (2023). Characterization and in vitro evaluation of hydroxyapatite from Fringescale Sardinella bones for biomedical applications. Journal of Saudi Chemical Society, 27(5), 101721.

Kjidaa, B., Mchich, Z., Saffaj, T., Saffaj, N., & Mamouni, R. (2024). Harnessing fish scales: Bio-hydroxyapatite and novel bio-hydroxyapatite@polypyrrole nanocomposite for advanced oxytetracycline antibiotic adsorption. Journal of Water Process Engineering, 68, 106515.

Kumar, C. S., Dhanaraj, K., Vimalathithan, R. M., Ilaiyaraja, P., & Suresh, G. (2021). Structural, morphological and anti-bacterial analysis of nanohydroxyapatite derived from biogenic (SHELL) and chemical source: Formation of apatite. Iranian Journal of Materials Science & Engineering, 18(1), 91-109.

Laonapakul, T., Sutthi, R., Chaikool, P., Talangkun, S., Boonma, A., & Chindaprasirt, P. (2021). Calcium phosphate powders synthesized from $CaCO_3$ and CaO of natural origin using mechanical activation in different media combined with solid-state interaction. Materials Science and Engineering: C, 118,

https://doi.org/10.24191/jmeche.v22i3.6477

111333.

Londoño-Restrepo, S. M., Millán-Malo, B. M., Del Real-López, A., & Rodriguez-García, M. E. (2019). In situ study of hydroxyapatite from cattle during a controlled calcination process using HT-XRD. Materials Science and Engineering: C, 105, 110020.

Mardziah, C. M., Ramesh, S., Tan, C. Y., Chandran, H., Sidhu, A., Krishnasamy, S., & Purbolaksono, J. (2021). Zinc-substituted hydroxyapatite produced from calcium precursor derived from eggshells. Ceramics International, 47(23), 33010-33019.

Mesri, M., Shamsudin, Z., Dom, A. H. M., Hassan, R., & Mulyadi, M. (2023). Experimental and validation of glass-ceramic composite properties derived from waste materials at elevated sintering temperature. Journal of Advanced Manufacturing Technology, 17(3), 1-12.

Mohd Pu'ad, N. A. S., Koshy, P., Abdullah, H. Z., Idris, M. I., & Lee, T. C. (2019). Syntheses of hydroxyapatite from natural sources. Heliyon, 5(5), e01588.

Mohd Pu'ad, N.A. S., Abdul Haq, R. H., Mohd Noh, H., Abdullah, H. Z., Idris, M. I., & Lee, T. C. (2020). Synthesis method of hydroxyapatite: A review. Materials Today: Proceedings, 29(1), 233–239.

Mondal, S., Park, S., Choi, J., Vu, T. T. H., Doan, V. H. M., Vo, T. T., Lee, B., & Oh, J. (2023). Hydroxyapatite: A journey from biomaterials to advanced functional materials. Advances in Colloid and Interface Science, 321, 103013.

Ofudje, E. A., Rajendran, A., Adeogun, A. I., Idowu, M. A., Kareem, S. O., & Pattanayak, D. K. (2018). Synthesis of organic derived hydroxyapatite scaffold from pig bone waste for tissue engineering applications. Advanced Powder Technology, 29(1), 1-8.

Paul, S., Pal, A., Choudhury, A. R., Bodhak, S., Balla, V. K., Sinha, A., & Das, M. (2017). Effect of trace elements on the sintering effect of fish scale derived hydroxyapatite and its bioactivity. Ceramics International, 43(17), 15678-15684.

Radulescu, D. E., Vasile, O. R., Andronescu, E., & Ficai, A. (2023). Latest research of doped hydroxyapatite for bone tissue engineering. International Journal of Molecular Sciences, 24(17), 13157.

Rahavi, S. S., Ghaderi, O., Monshi, A., & Fathi, M. H. (2017). A comparative study on physicochemical properties of hydroxyapatite powders derived from natural and synthetic sources. Russian Journal of Non-Ferrous Metals, 58(3), 276-286.

Ramesh, S., Loo, Z. Z., Tan, C. Y., Chew, W. J. K., Ching, Y. C., Tarlochan, F., Chandran, H., Krishnasamy, S., Bang, L. T., & Sarhan, A. A. D. (2018). Characterization of biogenic hydroxyapatite derived from animal bones for biomedical applications. Ceramics International, 44(9), 10525-10530.

Sunil, B. R., & Jagannatham, M. (2016). Producing hydroxyapatite from fish bones by heat treatment. Materials Letters, 185, 411-414.

Toibah, A. R., Misran, F., Shaaban, A., & Mustafa, Z. (2019). Effect of pH condition during hydrothermal synthesis on the properties of hydroxyapatite from eggshell waste. Journal of Mechanical Engineering and Sciences, 13(2), 4958-4969.

https://doi.org/10.24191/jmeche.v22i3.6477